Diagn Interv Radiol 2022; 28:39–49

© Turkish Society of Radiology 2021

CHEST IMAGING

ORIGINAL ARTICLE

Thoracic CT radiomics analysis for predicting synchronous brain metastasis in patients with lung cancer

Zhimin Ding
Yuancheng Wang
Cong Xia
Xiangpan Meng
Qian Yu
Shenghong Ju

PURPOSE

We aimed to assess the feasibility of radiomics analysis based on non-contrast-enhanced thoracic CT images in predicting synchronous brain metastasis (SBM) in lung cancer patients at initial diagnosis.

METHODS

This retrospective study enrolled 371 lung cancer patients (with SBM n=147, without SBM n=224) confirmed by histopathology. Patients were allocated to the training set (n=258) and testing set (n=113). The optimal radiomics features were selected by using the least absolute shrinkage and selection operator (LASSO) algorithm. The radiomics, clinicoradiologic, and combined models were developed to predict SBM using multivariable logistic regression. Then the discrimination ability of the models was assessed. Furthermore, the prediction performance of the abovementioned three models for oligometastatic (1-3 lesions) or multiple (>3 lesions) brain metastases in SBM, metachronous brain metastasis (MBM), and total (SBM and MBM) groups were investigated.

RESULTS

Six radiomics features and two clinicoradiologic characteristics were chosen for predicting SBM. Both the radiomics model (area under the receiver operating characteristic curve [AUC] = 0.870 and 0.824 in the training and testing sets, respectively) and the combined model (AUC = 0.912 and 0.859, respectively) presented better predictive ability for SBM than the clinicoradiologic model (AUC = 0.712 and 0.692, respectively). The decision curve analysis (DCA) demonstrated the clinical usefulness of the radiomics-based models. The radiomics model can also be used to predict oligometastatic or multiple brain metastases in SBM, MBM, and total groups ($P = .045$, $P = .022$, and $P = .030$, respectively).

CONCLUSION

The radiomics model and the combined model can be used as valuable imaging markers for predicting patients at high risk of SBM at the initial diagnosis of lung cancer. Furthermore, the radiomics model can also be utilized as an indicator for identifying oligometastatic or multiple brain metastases.

Lung cancer is the second most common primary malignant tumor, representing about 11.4% of cancer diagnoses in the world in 2020, and it is the leading cause (about 18%, i.e., 1.8 million) of cancer-related deaths worldwide,[1] of which distant metastases is the foremost reason.[2] The brain is the most commonly involved metastatic organ in patients with lung cancer.[3] As the most common primary cancer of brain metastasis (BM),[4,5] lung cancer accounts for more than 50% of BMs.[6] Among the primary tumors with brain metastasis at the initial diagnosis (i.e., synchronous brain metastasis, SBM), lung cancer accounted for 75.4% in a study on 2682 synchronous cases,[7] and 78% in another report.[8] About 10%-20% of non-small cell lung cancer (NSCLC) patients had BM at the initial diagnosis, and approximately 40% developed BM which was not found at diagnosis and revealed during the clinical course (i.e., metachronous brain metastasis, MBM) throughout the course of disease, with poor prognosis of about 3-6 months of overall survival.[9-11] SBMs were detected more frequently in small cell lung cancer (SCLC) and were diagnosed in about 24% of patients, and the accumulated occurrence of BM was around 50% at 2 years in SCLC.[12]

From the Department of Radiology (Z.D., Y.W., C.X., X.M., Q.Y., S.J. ✉ *jsh0836@hotmail.com*), Jiangsu Key Laboratory of Molecular and Functional Imaging, Zhongda Hospital, Medical School of Southeast University, Nanjing, China; Department of Radiology (Z.D.), Yijishan Hospital of Wannan Medical College, Wuhu, China.

Received 29 June 2021; revision requested 16 August 2021; last revision received 20 October 2021; accepted 29 November 2021.

Published online 29 December 2021.

DOI 10.5152/dir.2021.21677

You may cite this article as: Ding Z, Wang Y, Xia C, Meng X, Yu Q, Ju S. Thoracic CT radiomics analysis for predicting synchronous brain metastasis in patients with lung cancer. *Diagn Interv Radiol*. 2022;28(1):39-49.

It is crucially important to differentiate SBM from non-SBM because of different treatment strategies and prognoses. But some patients with SBM complained of mild or no clinical symptoms of the central nervous system,[8,13] therefore, further investigation of the brain in these patients were often delayed or overlooked. Although the guidelines of the 8th edition of the American Joint Committee on Cancer (AJCC) cancer staging recommend cranial MRI examination in the initial assessment of stages III-IV NSCLC,[14] and the National Comprehensive Cancer Network (NCCN) recommend staging cranial MRI in the initial assessment of stages II-IV NSCLC.[15] It is a tremendous burden on the healthcare system and economy to screen all potential SBM patients of lung cancer. It may be infeasible to perform MRI for all patients in resource-limited institutions, especially in underdeveloped countries. Furthermore, not all patients can perform MRI examination because of contraindications for MRI or contrast medium.

Based on its excellent density and spatial resolution, computed tomography (CT) has become the first choice diagnostic tool for lung disease. But the differential ability based on conventional radiological characteristics of thoracic CT is limited because of overlapping of these characteristics in lung cancer patients with and without SBM, and imperceptible differences of some potential features are impossible to be identified by naked eye. As an emerging technology for image analysis, radiomics can transform medical images into quantitative data noninvasively, and reflect the heterogeneity of tumors indirectly.[16] Nowadays, radiomics is used for predicting therapeutic effects, histological subtypes, and distant metastasis in lung cancer.[17-19] We hypothesized that the micro-environment of lung cancer changes in patients who have SBM, and radiomics analysis can be used to potentially complement recommended staging brain MRI examination by AJCC and NCCN. It can help to screen and improve personalized treatment options with thoracic CT images of lung cancer noninvasively and without additional costs. At the same time, number of BMs was also a significant prognostic factor for lung cancer patients.[20] Oligometastatic (1-3 lesions) or multiple (>3 lesions) BMs mean different therapeutic options and prognoses. Surgical resection or stereotactic radiosurgery was recommended to well-selected patients with oligometastatic BMs.[9,21]

In this article, we aim to evaluate whether the non-contrast-enhanced thoracic CT radiomics-based models can predict SBM in patients with lung cancer at initial diagnosis, and to assess whether these models can be used to predict oligometastatic or multiple BMs for further therapeutic selection in clinical practice.

Main points

- A radiomics analysis based on non-contrast-enhanced thoracic CT can be useful to predict the risk of synchronous brain metastasis (SBM) in patients with lung cancer at the initial diagnosis.
- Our study selected two clinicoradiologic factors and integrated them with the radiomics model to construct a nomogram presenting better performance than the radiomics model or clinicoradiologic model alone for predicting the risk of SBM.
- The radiomics model can also help identify oligometastatic (1-3 lesions) or multiple (>3 lesions) brain metastases.

Methods

Patients

This retrospective research was granted by the Institutional Review Board of our institution (No. 2020-188), who did not require informed consent of participants. In total, 681 cases with histopathologically confirmed lung cancer by biopsy or surgical removal from October 2012 to August 2020 were collected. Patients who underwent pretreatment chest CT and brain MRI examinations were recruited. The inclusion criteria were: 1) all cases confirmed with definite histopathological reports; 2) thoracic CT scans performed before biopsy or surgery; 3) plain and contrast-enhanced head MRI examinations performed within 2 weeks of thoracic CT scan. The exclusion criteria were: 1) biopsy or therapeutic history before thoracic CT examination; 2) unavailable pathological records or image data; 3) unsatisfactory resolution of thoracic CT images or lesions smaller than 1 cm, which did not allow for accurate delineation of the tumor and extraction of features. SBMs were diagnosed by pathology (neurosurgical resection, n=28; biopsy, n=11) or typical radiological features and follow-up examination (the suspicious brain metastasis progressed in number or size or decreased after chemotherapy or targeted therapy). The patients without SBMs were diagnosed by no evidence of BM through MRI examinations of the head or no suspicious BM during follow-up. Finally, 371 cases, 147 with SBM and 224 without SBM, were included. All 371 cases were allocated to the training set (n=258) and testing set (n=113) randomly, keeping the distribution of SBM and non-SBM cases in two sets consistent. The workflow of this study is shown in Figure 1.

Image acquisition

All cases had chest scan with a dual-source 64-multidetector CT (MDCT) (Somatom Definition Flash, Siemens Healthineers) or a 64-MDCT (Brilliance, Philips Healthcare) scanner. The CT protocol was as follows: tube current 140-250 mAs, tube voltage 120 kVp; slice thickness 5 mm; reconstruction section thickness 1.25 mm. Contrast-enhanced CT scans were performed after injection of iodinated contrast agent (1.0 mL/kg iohexol injection, 300 mg/mL, Omnipaque, GE Healthcare) at a rate of 3.5 mL/s via a pump injector through the antecubital vein. Some peripheral lung cancer patients (n=35) with typical CT characteristics were performed with only plain scans because there were no difficulties to confirm the boundary of lesions. All patients also underwent plain and contrast-enhanced brain MRI scan at a 3.0 T scanner (Signa HDXt, GE Healthcare) within 2 weeks of chest CT scan. Plain and contrast-enhanced brain MRI were performed as a routine follow-up examination every 3 months or when patients had neurologic symptoms. The detailed parameters of brain MRI are described in Supplementary Material 1.

Tumor segmentation, features extraction, selection and radiomics model building

ITK-SNAP software (version 3.6.0; www.itksnap.org) was utilized to segment volume of interest (VOI) from the lung lesions. To avoid the influence of adjacent normal tissue or secondary changes (i.e., atelectasis or postobstructive pneumonitis), contouring was delineated manually around the lesions carefully slice by slice in the cross-sectional images of plain CT by two board-certified radiologists (reader 1 and 2, with 5 and 10 years of experience in lung disease, respectively), using contrast-enhanced images as references. Reader 1 performed VOI segmentation of lesions in all 371 patients. After one month washout period to eliminate recall bias, reader 1 and reader 2 re-segmented VOI independently in 40 patients who were randomly chosen from the 371 patients. We selected the dedicated Artificial Intelligence Kit program (AK,

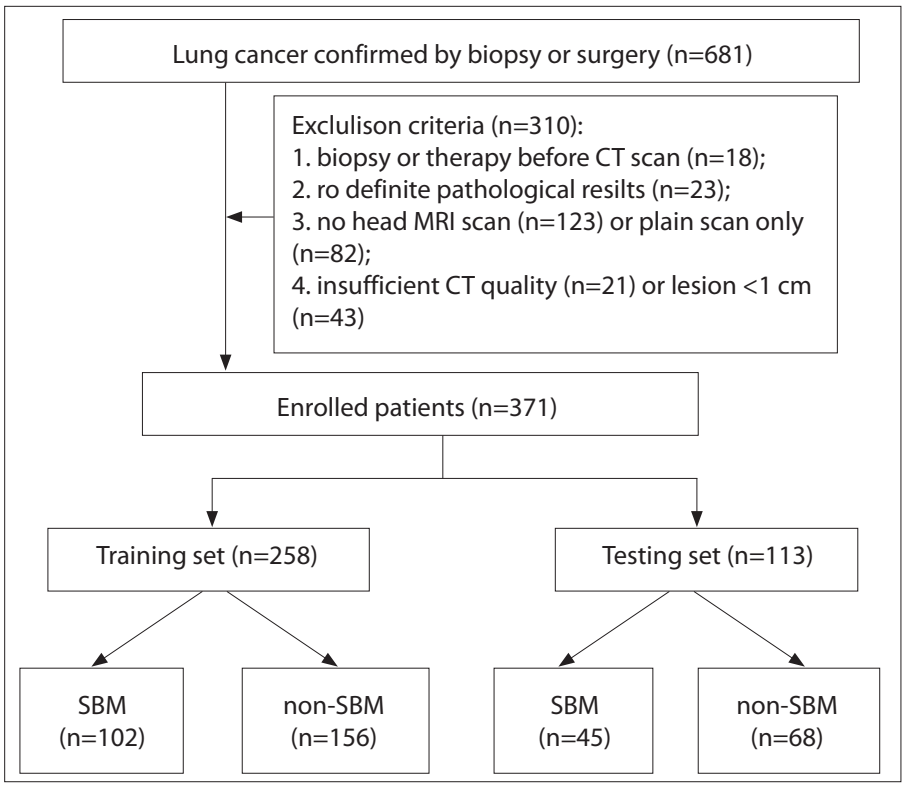

Figure 1. Workflow of this study. BM, brain metastasis; SBM, synchronous brain metastasis; MBM, metachronous brain metastasis.

Version: 3.2.0.R, GE Healthcare) to extract radiomics features. To eliminate the influence of different scanning parameters and scanners, resampling strategy (voxel size of 1×1×1 mm using a linear interpolation algorithm) was adopted in images and VOIs before feature extraction. All features of radiomics were standardized with Z-score normalization. The inter- and intra-observer consistency of feature extraction was evaluated using inter- and intra-class correlation coefficients (ICCs). The features with ICCs >0.8 were considered to be good consistency, and entered into the least absolute shrinkage and selection operator (LASSO) algorithm for feature dimension reduction. Then univariate logistic regression was performed to choose the features with $P < .05$. The radiomics model was built in the training set with the retained features using multivariable logistic regression and 5-fold cross-validation. Subsequently, the model was validated in an independent testing set. The score of the radiomics model (Rad-score) was computed for all 371 patients based on the selected features and weighted by their corresponding coefficients. SBM and non-SBM were entered into the model as 1 and 0, respectively. Mann-Whitney *U* test was performed to analyze the statistical differences of Rad-score between the two sets as well as the two groups (i.e., SBM group and non-SBM group) in each set.

Clinicoradiologic model construction

Baseline clinical and CT characteristics of patients were interpreted retrospectively by reader 1 and 2 independently blinded to clinical and pathological results. In cases where the two radiologists could not reach a consensus, a third experienced chest radiologist (19 years of experience) gave the final diagnosis. T and N stages were assigned according to the 8th edition of AJCC for lung cancer. In the training set, the differences of clinicoradiologic factors between lung cancer patients with and without SBM were analyzed, and the characteristics with $P < .05$ were selected into the multivariable logistic regression to analyze and construct a clinicoradiologic model. This model was then validated in the testing set.

Combined model and nomogram establishment and validation

Rad-score and clinicoradiologic characteristics ($P < .05$ in the univariate analyses) were selected as inputs. Multivariable logistic regression analysis was used to confirm the independent predictors and build a combined model for predicting SBM in the training set. The discriminative abilities of the three models were analyzed by area under the receiver operating characteristic curve (AUC). The performances and generalizability of the models were validated in the testing set. To differentiate SBM from non-SBM more conveniently, a nomogram derived from the combined model was developed in the training set. The calibration curves were used to evaluate the agreement between the predictions of SBM and the actual outcomes. The goodness-of-fit of the nomogram was evaluated using the Hosmer-Lemeshow test. The net benefits and clinical usefulness of the nomogram at different threshold probabilities were assessed by decision curve analysis (DCA).

Analysis based on the number of BMs in the SBM, MBM, and total groups

According to the number of metastatic brain lesions, BMs were divided into oligometastatic (1-3 lesions) and multiple BMs (more than 3 lesions).[13,22] Furthermore, the prediction ability of the aforementioned radiomics model, clinicoradiologic model, and combined model in differentiating oligometastatic from multiple BMs were analyzed based on patients in the SBM, MBM, and total (SBM and MBM) groups, respectively.

Statistical analysis

Statistical analysis and graphics were performed in SPSS 22.0 (IBM Corp.) and R software (open-source version 3.0.1, http://www.Rproject.org). Continuous variables were compared with Mann-Whitney *U* test or Student *t* test. Chi-square test was used to compare the categorical variables. The AUC was implemented to analyze the discrimination ability of the models. The differences in AUC values between models were evaluated using the Delong test. Lasso was performed using the "glmnet" package. Nomogram and calibration curve were developed using the "rms" package. DCA was drawn using the "rmda" package. A two-sided $P < .05$ was deemed to be a statistically significant difference.

Results

In total, 371 patients were included in our study (female: male, 115: 256; mean age, 63.15 ± 9.65 years; range, 34-90 years) and were classified into the SBM group (n=147)

and non-SBM group (n=224). The clinicopathological and radiological characteristics of patients in the training and testing sets are presented in Table 1. There were no statistically significant differences in the two sets. Associations of these characteristics between the SBM and non-SBM groups in two sets are summarized in Table 2.

Through the reproducibility assessment, 1088 of 1322 radiomics features with ICCs > 0.8 were identified. Features dimension reduction was performed using the LASSO algorithm in the training set, and the most distinguishable 19 features were left (Supplementary Figure S1). Eventually, 6 features with $P < .05$ were selected after univariate logistic regression analysis. The multivariate logistic regression was performed to build the radiomics model. The Rad-score was obtained by computing the 6 selected features via a linear formula for all 371 patients and presented as follows:

Rad-score = −0.9535 + 0.3296 × wavelet-HLH_gldm_Large Dependence Low Gray Level Emphasis + 0.1915 × wavelet-LHH_gldm_Large Dependence Low Gray Level Emphasis − 0.8466 × lbp-3D-m2_gldm_Dependence Variance + 0.1163 × log-sigma-3-0-mm-3D_firstorder_Maximum − 1.3012 × wavelet-LLH_glszm_Small Area Emphasis + 1.7032 × wavelet-HLH_glszm_Zone Entropy.

The Rad-score showed significant association with the risk of SBM in whole set (median, 0.56 for SBM group vs. -1.79 for non-SBM group, $P < .001$). SBM patients had a higher Rad-score than non-SBM in both sets (median, 0.64 vs. -1.87 and median, 0.56 vs. -1.42, both $P < .001$) (Table 2). The Rad-score demonstrated good predictive ability in differentiating SBM from non-SBM with AUCs of 0.870 (95% CI 0.828, 0.911) in the training set and 0.824 (95% CI 0.750, 0.898) in the testing set (Figure 2, Table 3).

Pathological subtype (adenocacinoma vs. non-adenocacinoma), CT reported T staging, and CT reported N staging (short axis of lymph node of hilar of pulmonary and/or mediastinum >1 cm was defined as positive) had significant difference between the two groups, SBM was more frequently observed in adenocarcinoma than in non-adenocarcinoma subtypes of lung cancer patients in both sets ($P = .010$ and $P = .030$, respectively). Patients with SBM had an incidence of higher CT reported T and N staging than without SBM in two sets ($P = .006$, $P = .040$ in CT reported T staging, and $P < .001$, $P = .012$ in CT reported N staging, respectively). After multivariable logistic

Table 1. Baseline characteristics of patients in training and testing set (n = 371)

Characteristics	Training set (n = 258)	Testing set (n = 113)	*P*
Clinical characteristics			
Sex, n (%) (Male / Female)	173 (67.1) / 85 (32.9)	83 (73.5) / 30 (26.5)	0.20
Age (years)[a]	62.51 ± 9.44	64.59 ± 9.99	0.056
NSCLC / SCLC, n (%)	222 (86.1) / 36 (13.9)	94 (83.2) / 19 (16.8)	0.48
Pathological subtype, n (%)			0.45
Adenocarcinoma	168 (65.1)	69 (61.1)	
Non-adenocarcinoma	90 (34.9)	44 (38.9)	
Radiographic characteristics			
Size (cm, range)	3.19 (1.08, 9.00)	3.44 (1.04, 8.22)	0.24
Plain CT scan values (HU)[a]	33.48 ± 7.77	34.98 ± 7.24	0.082
CT-reported T staging (T1[§] / T2 / T3 / T4)	75 / 115 / 34/ 34	28 / 47 / 24 / 14	0.26
CT-reported N staging (N0 / N1 / N2 / N3)	130 / 20 / 67 / 41	42 / 15 / 36 / 20	0.084
Central / peripheral lung cancer, n (%)	111 (43.1) / 147 (56.9)	57 (50.4) / 56 (49.6)	0.19
Lobulation, n (%) (Yes / No)	207 (80.2) / 51 (19.8)	93 (82.3) / 20 (17.7)	0.64
Spiculation, n (%) (Yes / No)	119 (46.1) / 139 (53.9)	54 (47.8) / 59 (52.2)	0.77
Pleural indentation, n (%) (Yes / No)	111 (43.1) / 147 (56.9)	48 (42.5) / 65 (57.5)	0.92
Pleural effusion, n (%) (Yes / No)	61 (23.6) / 197 (76.4)	24 (21.2) / 89 (78.8)	0.61
SBM, n (%)			0.96
With-SBM	102 (39.5)	45 (39.8)	
Without- SBM	156 (60.5)	68 (60.2)	
Rad-score, median (IQR)	−0.59 (−2.29, 0.70)	−1.71 (−2.33, 0.58)	0.79
Nomo-score, median (IQR)	−0.81 (−2.92, 0.95)	−0.42 (−3.06, 1.24)	0.75

SCLC, small cell lung cancer; NSCLC, non-small cell lung cancer; SBM, synchronous brain metastasis; Rad-score, radiomics score; Nomo-score, the score of nomogram derived from the combined model; HU, hounsfield unit.
[a]Data were presented as mean ± standard deviation; T1[§] (T1b+T1c).

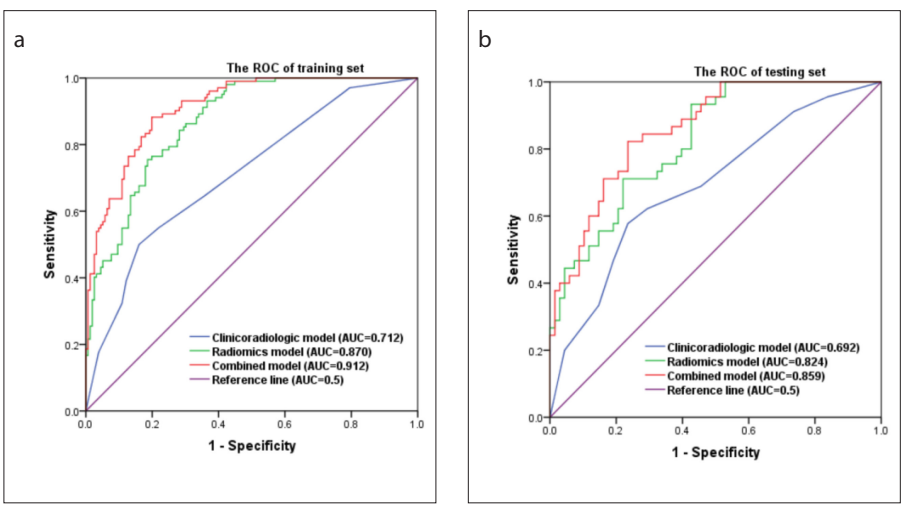

Figure 2. a, b. Receiver operating characteristic (ROC) curves of the clinicoradiologic model, radiomics model, and combined model in the training set **(a)** and testing set **(b)**. The predictive performance of the radiomics model and the combined model for synchronous brain metastasis were better than the clinicoradiologic model in both sets, and the combined model presented the best predictive performance in both sets.

Table 2. Comparison of baseline characteristics of patients in training and testing set between SBM group and non-SBM group (n=371)

	Training set (n = 258)			Testing set (n = 113)		
	SBM (n=102)	non-SBM (n=156)	*P*	SBM (n=45)	non-SBM (n=68)	*P*
Clinical characteristics						
Sex (M/F), n (%)	68 (66.7)/ 34 (33.3)	105 (67.3)/ 51 (32.7)	.83	29 (64.4)/ 16 (35.6)	54 (79.4)/ 14 (20.6)	.078
Age (years), mean±SD	63.00 ± 8.75	62.19 ± 9.88	.50	63.87 ± 9.13	65.07 ± 10.57	.53
NSCLC or SCLC, n (%)			.17			.82
NSCLC	84 (82.4)	138 (88.5)		37 (82.2)	57 (83.8)	
SCLC	18 (17.6)	18 (11.5)		8 (17.8)	11 (16.2)	
Pathological subtype, n (%)			.010[a]			.030[a]
Adenocarcinoma	76 (74.5	92 (59.0)		33 (73.3)	36 (52.9)	
Non-adenocarcinoma	26 (25.5)	64 (41.0)		12 (26.7)	32 (47.1)	
Radiographic characteristics						
Size (cm), median (range)	3.42 (1.50, 9.00)	3.07 (1.08, 7.94)	.085	3.56 (1.43, 8.22)	3.26 (1.04, 7.82)	.31
Plain CT scan values (HU), mean±SD	33.56 ± 8.05	33.43 ± 7.61	.89	34.36 ± 8.21	35.39 ± 6.56	.46
CT-reported T staging (T1[§]/T2/T3/T4)	26/38/16/22	49/77/18/12	.006[a]	8/16/11/10	20/31/13/4	.040[a]
CT-reported N staging (N0/N1/N2/N3)	34/7/32/29	96/13/35/12	< .001[b]	12/4/15/14	30/11/21/6	.012[a]
Central or peripheral lung cancer, n (%)			.59			.16
Central	46 (45.1)	65 (41.7)		19 (42.2)	38 (55.9)	
Peripheral	56 (55.9)	91 (58.3)		26 (57.8)	30 (44.1)	
Pleural effusion, n (%)	26 (25.5)	35 (22.4)	.57	9 (20.0)	25 (36.8)	.79
Lobulation, n (%)	85 (83.3)	122 (78.2)	.31	38 (84.4)	55 (80.9)	.63
Speculation, n (%)	52 (51.0)	67 (42.9)	.21	25 (55.6)	29 (42.6)	.18
Pleural indentation, n (%)	51 (50.0)	60 (38.5)	.067	22 (48.9)	26 (38.2)	.26
Rad-score, median (IQR)	0.64 (−0.05, 1.69)	−1.87 (−3.64, −0.30)	< .001[b]	0.56 (−0.25, 1.21)	−1.42 (−4.45, 0.09)	< .001[b]
Nomo-score, median (IQR)	1.31 (0.08, 2.70)	−2.47 (−4.72, −0.83)	< .001[b]	1.24 (−0.09, 2.34)	−2.24 (−5.07, −0.26)	< .001[b]

T1[§] (T1b+T1c); [a]*P* < .05; [b]*P* < .001.
SCLC, small cell lung cancer; NSCLC, non-small cell lung cancer; SBM, synchronous brain metastasis; Rad-score, radiomics score; Nomo-score, the score of nomogram derived from the combined model.

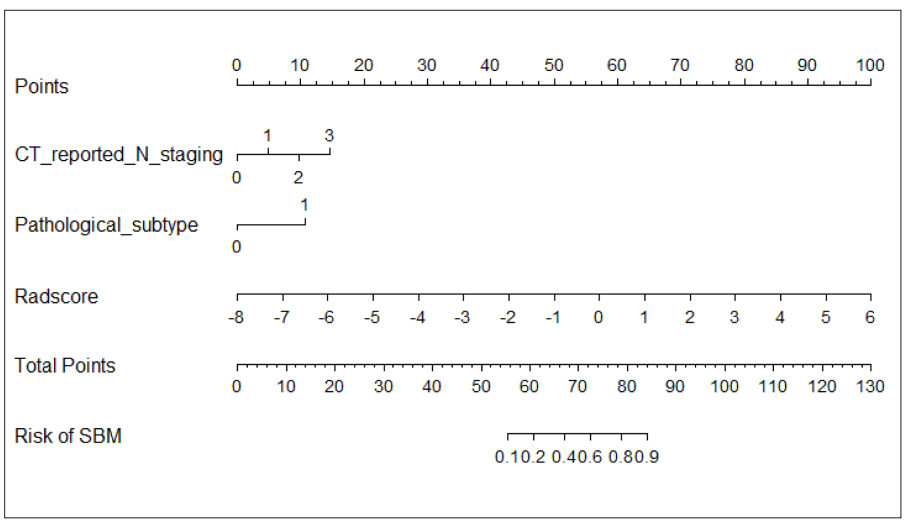

Figure 3. The nomogram for the prediction of SBM in lung cancer patients. The nomogram was constructed by incorporating the CT reported N staging, pathological subtype (0, non-adenocarcinoma; 1, adenocarcinoma) and Rad-score. The sum of the scores on the scoring ruler corresponding to the three predictors is the total score, and the scale values of the upper ruler corresponding to the total score are the risk of SBM.

regression analysis, CT reported N staging and pathological subtype were confirmed as independent predictive factors. The clinicoradiologic model was constructed in the training set (AUC = 0.712) and validated in the testing set (AUC = 0.692).

By incorporating Rad-score and the selected clinicoradiologic features (pathological subtype and CT reported N staging), the combined model displayed good prediction efficacy in both sets (Figure 2, Table 3). The Delong test revealed that there was no difference between the radiomics model and the combined model (*P* = .12 and *P* = .49 in two sets, respectively), but both models presented better predictive ability for SBM than the clinicoradiologic model (both *P* < .001 in the training set; *P* = .038 for radiomics model vs. clinicoradiologic model and *P* = .006 for combined model vs. clinicoradiologic model in the testing set) (Supplementary Table

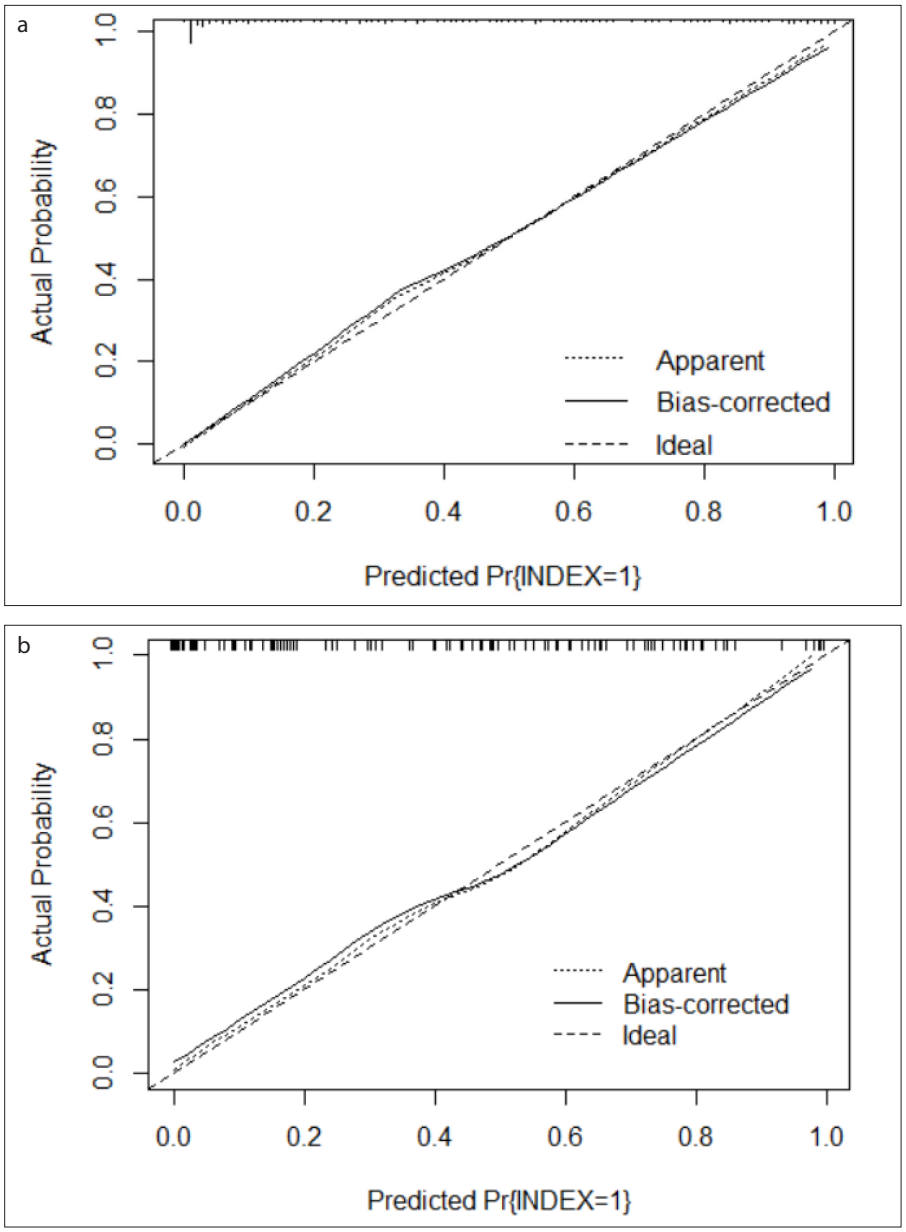

Figure 4. a, b. Calibration curves of the nomogram in the training set **(a)** and testing set **(b)**. The calibration curves show the calibration of the nomogram in terms of agreement between the predicted probability of SBM and actual outcomes. The 45° line indicates perfect prediction, and the curve lines indicate the predictive performance of the nomogram. The closer the lines, the better predictive accuracy of the nomogram.

Table 3. Predictive performance of the clinicoradiologic, radiomics, and combined models for the risk of SBM in the training and testing sets

Variables		AUC	(95% CI)	Accuracy	Sensitivity	Specificity
CR model	Training set	0.712	(0.648-0.776)	0.643	0.647	0.641
	Testing set	0.692	(0.592-0.792)	0.602	0.689	0.544
Radiomics model	Training set	0.870	(0.828-0.911)	0.787	0.735	0.821
	Testing set	0.824	(0.750-0.898)	0.708	0.711	0.706
Combined model	Training set	0.912	(0.879-0.945)	0.833	0.882	0.801
	Testing set	0.859	(0.793-0.925)	0.814	0.844	0.676

SBM, synchronous brain metastasis; AUC, area under the receiver operating characteristic curve; CI, confidence interval; CR model, clinicoradiologic model.

S1). The combined model was visualized as a nomogram in the training set (Figure 3). The Nomo-score was obtained by calculating the formula of the combined model for all 371 patients, and presented significant association with the risk of SBM (median, 1.26 vs. -2.39, $P < .001$). SBM patients had a higher Nomo-score than non-SBM in the training set (median, 1.31 vs. -2.47, $P < .001$), which was verified in the testing set (median, 1.24 vs. -2.44, $P < .001$).

The calibration curves of the nomogram presented good agreement between predicted and actual probability of SBM in both sets (Figure 4). The Hosmer-Lemeshow test demonstrated no difference in both sets ($P = .71$ and $P = .53$, respectively), indicating that there were no departure from a perfect goodness-of-fit. The DCAs for the three models were graphically displayed in Figure 5, which indicated that the combined model and the radiomics model added more net benefits to predict SBM status than the clinicoradiologic model and treat-all or none scheme.

Overall, 147 patients were confirmed with SBM at the initial diagnosis of lung cancer. Eighty-nine patients were confirmed MBM in 149 non-SBM patients during follow-up, and median time from diagnosis of lung cancer to MBMs was 12 months (3-70 months). The median follow-up was 45 months (36-72 months) for 60 patients who did not have MBMs. Totally, 75 cases were lost to follow-up after the initial diagnosis. The number of BM patients in the total group was 236. The distribution of oligometastatic and multiple BMs in three groups were presented in Table 4. The Rad-score of oligometastatic BM patients were higher than the multiple ones in all the three groups (all $P < .05$) (Supplementary Figure S2). The clinicoradiologic model and Nomo-score of the combined model showed no statistical differences in all three groups ($P = .42$, $P = .19$ and $P = .20$, and $P = .10$, $P = .12$ and $P = .17$, respectively)

Discussion

In our study, we constructed and tested a radiomics model based on non-contrast-enhanced thoracic CT for prediction of SBM in lung cancer patients at the initial diagnosis, which presented good discrimination performance and clinical utility. By integrating the Rad-score and two clinicoradiologic risk factors (adenocarcinoma histology subtype and CT reported N staging), the combined model demonstrated more discrimination ability than the radiomics and clinicoradio-

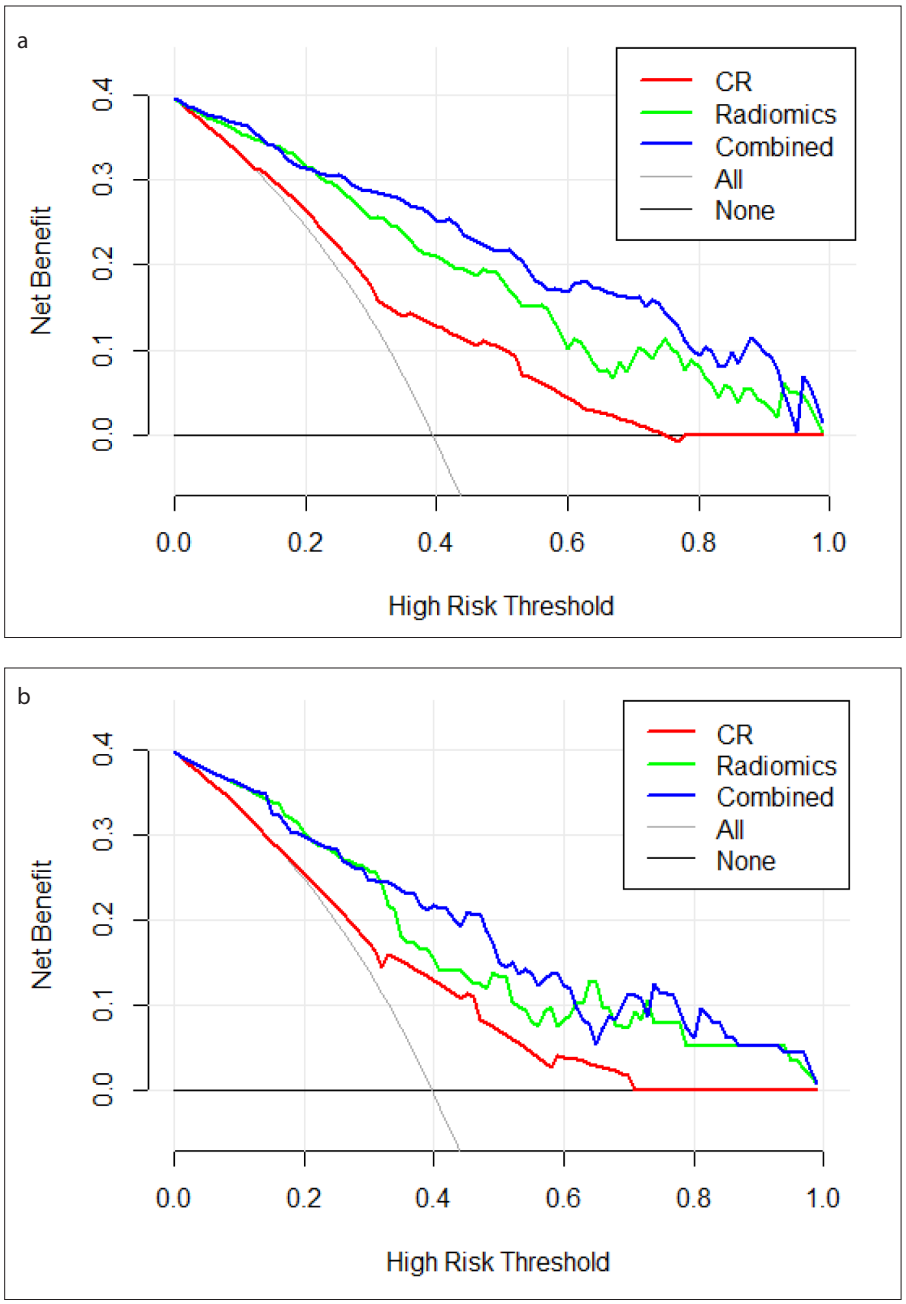

Figure 5. a, b. Decision curve analysis for the three models in the training set **(a)** and testing set **(b)**. The net benefit versus the threshold probability was plotted. The *thin gray* and *bold gray* lines represent the hypothesis that all lung cancer patients and no patients had synchronous brain metastasis, respectively. The net benefits of the combined model *(blue line)* and radiomics model *(green line)* were higher than the clinicoradiologic model *(red line)* across most ranges of threshold probability. CR, clinicoradiologic model.

logic models alone. The nomogram derived from the combined model can be used easily as a visualized and effective tool to predict the risk of SBM for a newly diagnosed lung cancer patient. Furthermore, we tried to use the abovementioned models to distinguish oligometastatic BMs from multiple ones, and found that only the radiomics model presented statistically significant differences.

Timely and accurate detection of SBM may alter the therapeutic strategy for lung cancer and enable timely therapy or cure of the BM. The presence of SBM means poor prognosis,[10,11] and needs more aggressive therapeutic methods for patients with lung cancer.[9,23] Radiomics can extract and analyze quantitative features from digital medical images and transform them into mineable data, which can assess heterogeneity of tumors. By analyzing these data, we can select the most useful radiomics features to improve the ability of diagnosis, prediction, stage, and so on.[24-26] Chen et al.[27] analyzed the maximum region of interest (ROI) of tumor in 89 category T1 lung adenocarcinoma patients and constructed the radiomics model with four selected features derived from pretreatment CT images. The model demonstrated good prediction ability for SBM (AUC = 0.847). But that model was only validated internally with a 10-fold cross-validation approach, without independent testing set because of the limited sample size. Also, some brain scans were performed with CT, which may lead to missed diagnosis of occult brain metastatic lesions. In our study, we used radiomics features derived from the 3D VOI of tumor to predict SBM in 371 lung cancer patients. Compared with 2D ROI, the 3D VOI can reflect the inherent heterogeneity of tumors more comprehensively and provide morphological information more completely. We built the radiomics model with 5-fold cross-validation in the training set (AUC = 0.870), and an independent testing set was used to validate the reproducibility and generalization of the model (AUC = 0.827). In our study, all patients underwent cranial MRI, as suggested by guidelines of AJCC and NCCN. Xu et al.[28] analyzed radiomics features extracted from lesions of pretreatment CT in 132 stage III-IV ALK positive NSCLC patients and confirmed only one feature can be used to predict SBM with AUC of 0.682 in the training set and 0.642 in the testing set. However, that research had a small sample size (only 27 cases had SBM in 132 patients) and modest predictive efficiency. Compared with that study, the radiomics model in our study was built with 6 selected radiomics features and showed higher risk prediction for SBM with AUCs of 0.870 and 0.824 in two sets. This may indicate that multiple features contain more characteristics of heterogeneity of tumor and the corresponding radiomics model is more suitable for SBM risk prediction of lung cancer. Therefore, it is more reliable to associate the heterogeneity and complex biological behavior of tumors with multi-features in radiomics studies.

In this study, we analyzed a set of clinicoradiologic factors that might help predict SBM of lung cancer patients. Only adenocarcinoma histology and CT reported N staging were finally selected as independent predictors to establish the clinicoradiologic model. Adenocarcinoma histology has

been reported to be one of the important independent risk factors for SBM.[29,30] In our study, the presence of adenocarcinoma histology was correlated closely with SBM of lung cancer, which was similar to previous studies.[29,30] Our study demonstrated that patients with higher CT reported N staging were more likely to have SBM. This might be interpreted as the risk of hematogenous metastasis of lung cancer being markedly related with increased lymph node stage, which means more aggressive biological characteristic.[31,32] However, our clinicoradiologic model only presented moderate discriminative ability, which may manifest that basic radiologic and clinicopathologic factors have inadequate predictive value and additional tools are needed to improve predictive ability of SBM in lung cancer.

By incorporating Rad-score, pathological subtype and CT reported N staging, the combined model was built and presented the best predictive efficiency in predicting SBM in three models in both the training and testing sets, which were confirmed by Delong test. Compared with the radiomics model, the combined model had relatively lower specificity in both sets, but its higher sensitivity was helpful to identify true SBM patients, and this was our main purpose, so the relative lower specificity was acceptable. The nomogram, which was derived from the combined model, could be utilized to help doctors to identify high risk patients with SBM who need a detailed examination of the brain. Calibration curves were established to show the performance of the nomogram for the differentiation of SBM and non-SBM. The curves presented favorable agreement between the observed and predicted values in both sets. DCA was utilized to evaluate the added value of the nomogram and the radiomics model in predicting SBM. It showed that the combined model can gain the most significant benefit in the three models in predicting SBM in lung cancer patients at most threshold probabilities, and the radiomics model had more net benefit than the clinicoradiologic model as well.

It is also important to identify oligometastatic or multiple BMs because of the different treatment strategies and prognoses. Patients with higher numbers of BMs have worse overall survival.[33] Oligometastatic BMs are associated with better response to surgical resection or stereotactic radiosurgery and better prognosis in selected patients.[9,20] But these treatments may not be suitable for multiple BMs, particularly diffuse lesions, which usually need whole-brain irradiation or target treatment. From the results of our study, we additionally found that the Rad-score can be used not only in evaluating the risk of SBM but also in predicting oligometastatic or multiple BMs synchronously and metachronously in lung cancer patients. So the radiomics model can act as a convenient indicator in clinical practice of management in lung cancer patients with BMs. But the clinicoradiologic model and the combined model were not useful in differentiating oligometastatic from multiple BMs in all three groups. The possible reason could be that the micro-environment and heterogeneity of lung cancer are different between the oligometastatic and multiple BMs. The clinicoradiologic factors cannot identify these intangible differences, but radiomics can interpret images more detailed and objective, and demonstrate quantitative information and heterogeneity of the tumor at a cellular level.

Our study has certain limitations. First, the research was a single-institution, retrospective analysis, and the sample size of cases was relatively small, which may lead to bias in patient selection and model instability. A larger sample size and multicenter study should be carried out in the future. Second, the features of radiomics were only extracted from the images of non-contrast-enhanced CT, which may cause the loss of some information compared with contrast-enhanced CT. But the unenhanced CT scan is the routine and cost-effective method in clinical practice of lung cancer diagnosis, and variability of different acquisition time or different phases from contrast-enhanced scan can be avoided. Third, some diagnoses of BM were not confirmed by pathological results but by typical radiological features and follow-up; however, this was considered reasonable and reliable in clinical practice.[29] Finally, considering that the brain is the most frequently metastatic organ of lung cancer and that BM has the most obvious influence on the prognosis and quality of life of the patients, our study only focused on patients who had BMs. The study of extracranial metastases should be included in future research.

In conclusion, the non-contrast-enhanced thoracic CT radiomics-based models can be utilized as cost-effective and noninvasive tools to assist clinicians in predicting the risk of SBM in lung cancer patients at initial diagnosis, especially in underdeveloped countries, and certain patients who are contraindicated for MRI examination. Furthermore, the radiomics

Table 4. The comparison of oligometastatic and multiple BMs in the SBM, MBM, and total groups of the three models

	CR model	Rad-score	Nomo-score
SBM			
Oligo- BM (n=52)	−0.327 (−0.796, 0.530)	0.829 (−0.016, 2.667)	1.767 (0.258, 3.258)
Multiple BM (n=95)	0.284 (−0.796, 0.530)	0.480 (−0.255, 1.240)	1.086 (−0.094, 2.488)
z	−0.810	−2.005	−1.641
P	.42	.045*	.10
MBM			
Oligo- BM (n=33)	−0.796 (−1.924, −0.688)	−0.553 (−3.778, 0.870)	−1.696 (−4.833,−0.285)
Multiple BM (n=56)	−0.796 (−0.796, −0.327)	−2.442 (−4.250,−0.915)	−3.024 (−5.038,−1.037)
z	−1.220	−2.149	−1.512
P	0.19	0.022*	0.12
Total			
Oligo- BM (n=85)	−0.688 (−0.796, 0.440)	0.106 (−0.710, 1.312)	0.448 (−1.603, 2.127)
Multiple BM (n=151)	−0.688 (−0.796, 0.530)	−0.051 (−1.535, 0.852)	0.101 (−2.055, 1.659)
z	−1.285	−2.166	−1.383
P	.20	.030*	.17

Data were presented as median (interquartile range).
BM, brain metastasis; SBM, synchronous brain metastasis; MBM, metachronous brain metastasis; CR model, clinicoradiologic model; Rad-score, radiomics score; Nomo-score, the score of nomogram derived from the combined model; Oligo-, oligometastatic; Total, SBM+MBM.
*$P < .05$.

model can also help to identify oligometastatic or multiple BMs, which may help in treatment decision-making.

Financial disclosure

This study was supported by the National Natural Science Foundation of China (Grant No. 81830053, 92059202), the Key Project of Scientific Research Fund of Wannan Medical College (Grant No. WK2019ZF05), and the Scientific Research Project of the Chinese Red Cross foundation (Grant No. XM_HR_YXFN_2021_05_24). The funders had no role in the study design, data collection and analysis, decision to publish, or preparation of the manuscript.

Conflict of interest disclosure

The authors declared no conflicts of interest.

References

1. Sung H, Ferlay J, Siegel RL, et al. Global cancer statistics 2020: GLOBOCAN estimates of incidence and mortality worldwide for 36 cancers in 185 countries. *Ca Cancer J Clin*. 2021;71:209-249. [Crossref]
2. Dragoj M, Milosevic Z, Bankovic J, et al. Targeting CXCR4 and FAK reverses doxorubicin resistance and suppresses invasion in non-small cell lung carcinoma. *Cell Oncol (Dordr)*. 2017;40:47-62. [Crossref]
3. Yang L, Li J, Fu S, et al. Up-regulation of insulin-like growth factor binding protein-3 is associated with brain metastasis in lung adenocarcinoma. *Mol Cells*. 2019;42:321-332.
4. Nolan C, Deangelis LM. Overview of metastatic disease of the central nervous system. *Handb Clin Neurol*. 2018;149:3-23. [Crossref]
5. Soffietti R, Cornu P, Delattre JY, et al. EFNS Guidelines on diagnosis and treatment of brain metastases: report of an EFNS Task Force. *Eur J Neurol*. 2006;13:674-681. [Crossref]
6. Budczies J, von Winterfeld M, Klauschen F, et al. The landscape of metastatic progression patterns across major human cancers. *Oncotarget*. 2015;6:570-583. [Crossref]
7. Thomas AJ, Rock JP, Johnson CC, et al. Survival of patients with synchronous brain metastases: an epidemiological study in southeastern Michigan. *J Neurosurg*. 2000;93:927-931. [Crossref]
8. Shibahara I, Kanamori M, Watanabe T, et al. Clinical Feature s of precocious, synchronous, and metachronous brain metastases and the role of tumor resection. *World Neurosurg*. 2018;113:e1-e9. [Crossref]
9. Ali A, Goffin JR, Arnold A, et al. Survival of patients with non-small-cell lung cancer after a diagnosis of brain metastases. *Curr Oncol*. 2013;20:e300-306. [Crossref]
10. Cagney DN, Martin AM, Catalano PJ, et al. Incidence and prognosis of patients with brain metastases at diagnosis of systemic malignancy: a population-based study. *Neuro Oncol*. 2017;19:1511-1521. [Crossref]
11. Sánchez de Cos J, Sojo González MA, Montero MV, et al. Non-small cell lung cancer and silent brain metastasis. Survival and prognostic factors. *Lung Cancer*. 2009;63:140-145. [Crossref]
12. Hochstenbag MM, Twijnstra A, Wilmink JT, et al. Asymptomatic brain metastases (BM) in small cell lung cancer (SCLC): MR-imaging is useful at initial diagnosis. *J Neurooncol*. 2000;48:243-248. [Crossref]
13. Chen XR, Hou X, Li DL, et al. Management of non-small-cell lung cancer patients initially diagnosed with 1 to 3 synchronous brain-only metastases: a retrospective study. *Clin Lung Cancer*. 2020;22:e25-34. [Crossref]
14. Amin MB, Edge S, Greene F, et al, eds. AJCC Cancer Staging Manual. 8th ed. New York, NY: Springer, 2017. [Crossref]
15. National Comprehensive Cancer Network. Clinical Practice Guidelines in Oncology for non-small cell lung cancer. http://www.nccn.org. Published 2020. Accessed February 2020.
16. Gillies RJ, Kinahan PE, Hricak H. Radiomics: images are more than pictures, they are data. *Radiology*. 2016;278:563-577. [Crossref]
17. Zhang NS, Liang R, Gensheimer MF, et al. Early response evaluation using primary tumor and nodal imaging features to predict progression-free survival of locally advanced non-small cell lung cancer. *Theranostics*. 2020;10:11707-11718. [Crossref]
18. E LN, Lu L, Li L, et al. Radiomics for classifying histological subtypes of lung cancer based on multiphasic contrast-enhanced computed tomography. *J Comput Assist Tomogr*. 2019;43:300-306. [Crossref]
19. Coroller TP, Grossmann P, Hou Y, et al. CT-based radiomic signature predicts distant metastasis in lung adenocarcinoma. *Radiother Oncol*. 2015;114:345-50. [Crossref]
20. Sperduto PW, Chao ST, Sneed PK, et al. Diagnosis-specific prognostic factors, indexes, and treatment outcomes for patients with newly diagnosed brain metastases: a multi-institutional analysis of 4,259 patients. *Int J Radiat Oncol Biol Phys*. 2010;77:655-661. [Crossref]
21. Casiraghi M, Bertolaccini L, Sedda G, et al. Lung cancer surgery in oligometastatic patients: outcome and survival. *Eur J Cardiothorac Surg*. 2020;57:1173-1180. [Crossref]
22. Alhalabi O, Soomro Z, Sun R, et al. Outcomes of changing systemic therapy in patients with relapsed breast cancer and 1 to 3 brain metastases. *NPJ Breast Cancer*. 2021:28:1-5. [Crossref]
23. Lippitz B, Lindquist C, Paddick I, et al. Stereotactic radiosurgery in the treatment of brain metastases: the current evidence. *Cancer Treat Rev*. 2014;40:48-59. [Crossref]
24. Zhang Z, Jiang X, Zhang R, Yu T, Liu S, Luo Y. Radiomics signature as a new biomarker for preoperative prediction of neoadjuvant chemoradiotherapy response in locally advanced rectal cancer. *Diagn Interv Radiol*. 2021;27:308-314. [Crossref]
25. Banerjee S, Wang DS, Kim HJ, et al. A computed tomography radiogenomic biomarker predicts microvascular invasion and clinical outcomes in hepatocellular carcinoma. *Hepatology*. 2015;62:792-800. [Crossref]
26. Zhao ZR, Bian Y, Jiang H, et al. CT-radiomic approach to predict G1/2 nonfunctional pancreatic neuroendocrine tumor. *Acad Radiol*. 2020;27:e272-e281. [Crossref]
27. Chen AP, Lu L, Pu XH, et al. CT-based radiomics model for predicting brain metastasis in category T1 lung adenocarcinoma. *AJR Am J Roentgenol*. 2019;213:134-139. [Crossref]
28. Xu X, Huang L, Chen J, et al. Application of radiomics signature captured from pretreatment thoracic CT to predict brain metastases in stage III/IV ALK-positive non-small cell lung cancer patients. *J Thorac Dis*. 2019;11(11):4516-4528. [Crossref]
29. Kim M, Suh CH, Lee SM, et al. Diagnostic yield of staging brain MRI in patients with newly diagnosed non-small cell lung cancer. *Radiology*. 2020;297:419-427. [Crossref]
30. Naresh G, Malik PS, Khurana S, et al. Assessment of brain metastasis at diagnosis in non-small-cell lung cancer: a prospective observational study from North India. *JCO Glob Oncol*. 2021;7:593-601. [Crossref]
31. Waqar SN, Samson PP, Robinson CG, et al. Non-small-cell lung cancer with brain metastasis at presentation. *Clin Lung Cancer*. 2018;19:e373-e379. [Crossref]
32. Mujoomdar A, Austin JH, Malhotra R, et al. Clinical predictors of metastatic disease to the brain from non-small cell lung carcinoma: primary tumor size, cell type, and lymph node metastases. *Radiology*. 2007;242:882-888. [Crossref]
33. Gray PJ, Mak RH, Yeap BY, et al. Aggressive therapy for patients with non-small cell lung carcinoma and synchronous brain-only oligometastatic disease is associated with long-term survival. *Lung Cancer*. 2014;85:239-244. [Crossref]

Supplementary Material 1. The detailed parameters of MRI for head examination.

MR images were acquired with 3.0 T scanner (Signa HDXt, GE Healthcare) using a 8-channel phase-array head coil in the supine position, and consisted of six sequences including axial T2-weighted imaging (T2WI), T1 Fluid-attenuated inversion-recovery (FLAIR), T2 FLAIR, diffusion-weighted imaging (DWI) with two b-factors (0 and 1000 s/mm^2). Contrast-enhanced T1-weighted imaging (T1 WI) were performed in the axial, sagital and coronal planes. The detailed parameters of MRI sequences: T1 FLAIR, TI 800~900 ms, TR 2000~2500 ms, TE 20~25 ms; T2WI, TR 4000~4500 ms, TE 100~110 ms; T2 FLAIR, TI 2000~2100ms, TR 8000~8600 ms, TE 150~170 ms, FOV 240 mm × 240 mm, slice thickness 6 mm, slice interval 2 mm, matrix 256 × 256; DWI, TR 4500~5500 ms, TE 70~80ms, FOV 240 mm × 240 mm, slice thickness 6 mm, slice interval 2 mm, matrix 160 × 160. Contrast-enhanced scans were performed after injection of 0.01mmol/kg of Gd-DTPA contrast agent (gadobutrol, Bayer-Schering Pharma) at a rate of 2.0 mL/s with a pump injector (Ulrich CT Plus 150, Ulrich Medical) through the antecubital vein, followed by a saline flush (20 mL). The parameters of contrast-enhanced MRI sequences: sagittal high-resolution T1W1 3D BRAVO, TR 8.1 ms, TE 2.8 ms, FA 12°, slice thickness 0 mm, thickness 1 mm, 175 slices, voxel size 1 mm × 1 mm × 1 mm. T1 FLAIR, TI 800~900ms, TR 2000~2500ms, TE 20~25ms.

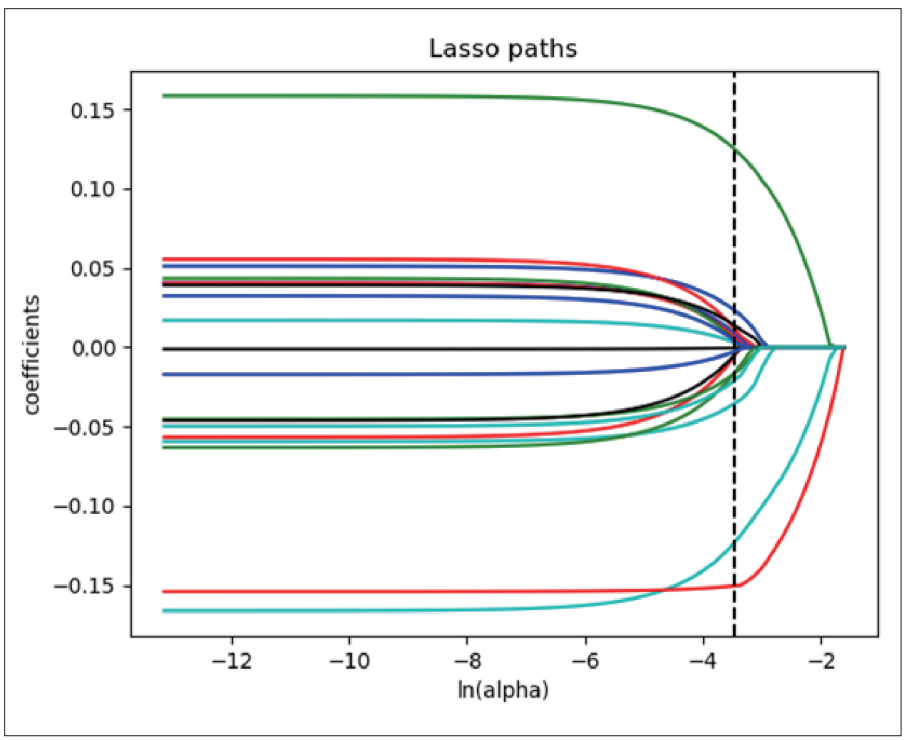

Supplementary Figure S1. LASSO path plot in the training set. Features dimension reduction was performed using the least absolute shrinkage and selection operator (LASSO) algorithm in the training set, and the most distinguishable 19 features were left.

Supplementary Table 1. Comparison of AUC values between models using Delong test in the training and testing sets

	CR model	Radiomics model	Combined model	
	AUC (95% CI)	AUC (95% CI)	AUC (95% CI)	*P*
Training set (n=258)	0.712 (0.648-0.776)	0.870 (0.828-0.911)	-	<.001[a]
	0.712 (0.648-0.776)	-	0.912 (0.879-0.945)	<.001[a]
	-	0.870 (0.828-0.911)	0.912 (0.879-0.945)	.12
Testing set (n=113)	0.692 (0.592-0.792)	0.824 (0.750-0.898)	-	.038[b]
	0.692 (0.592-0.792)	-	0.859 (0.793-0.925)	.006[b]
	-	0.824 (0.750-0.898)	0.859 (0.793-0.925)	.49

CR model, clinicoradiologic model; AUC, area under the receiver operating characteristic (ROC) curve; CI, Confidence interval.
[a]*P* < .001; [b]*P* < .05.

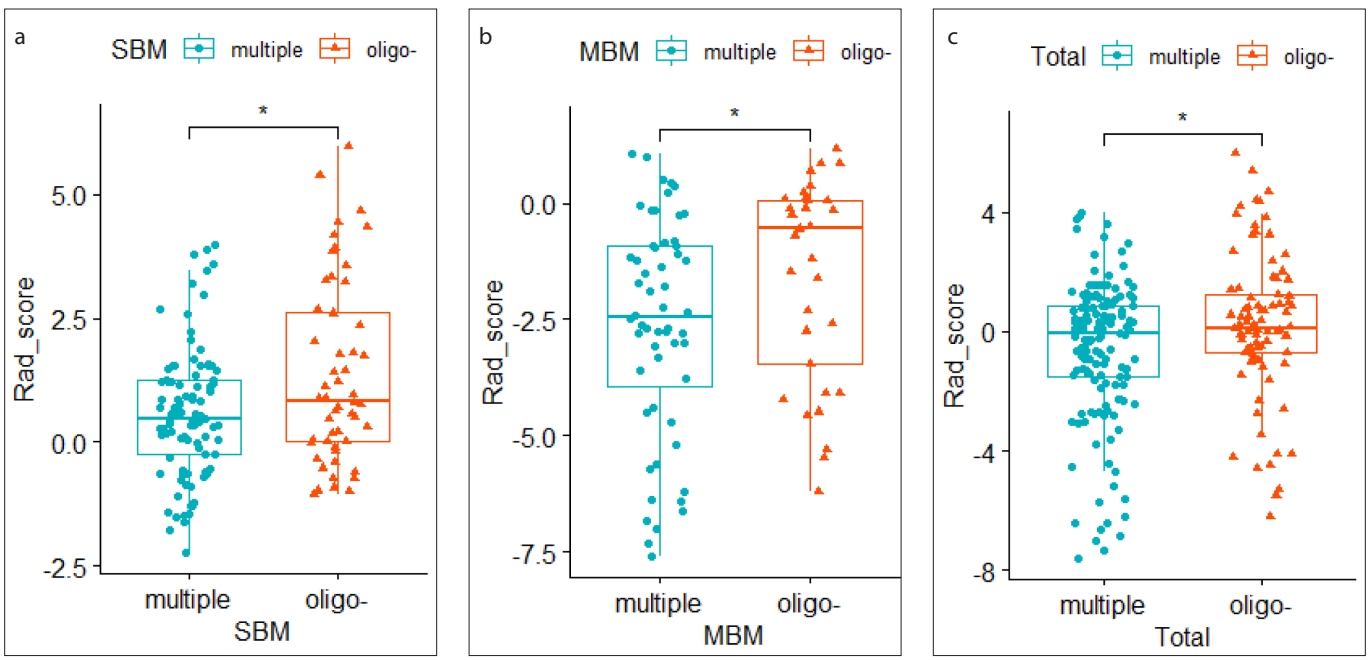

Supplementary Figure S2. a-c. The Rad-score of each patient in SBM group **(a)**, MBM group **(b)**, and total group **(c)**. The Mann-Whitney U test was used to evaluate the difference between the oligometastatic and multiple brain metastases. SBM, synchronous brain metastasis; MBM, metachronous brain metastasis; Total, SBM+MBM; Rad-score, radiomics score; *, *P* < .05.